Journal of Inorganic and General Chemistry
ZAAC
Zeitschrift für anorganische und allgemeine Chemie
www.zaac.wiley-vch.de
RESEARCH ARTICLE
DOI: 10.1002/zaac.202200118

The True Nature of $SmSb_2O_4Cl$: Syntheses and Crystal Structures of $Sm_2[Sb_4O_8]Cl_2$ and $Eu_2[Sb_4O_8]Cl_2$

Ralf J. C. Locke[a] and Thomas Schleid*[a]

Dedicated to Professor Caroline Röhr on the Occasion of her 60th Birthday

The two lanthanoid oxidoantimonate(III) chlorides $SmSb_2O_4Cl$ and $EuSb_2O_4Cl$ are accessible from solid-state reactions of Sb_2O_3 with Ln_2O_3 and $LnCl_3$ (Ln = Sm and Eu) at 750 °C for two days. They crystallize in the centrosymmetric tetragonal space group *P4/ncc* with the lattice parameters a = 787.13(4) pm, c = 1765.24(12) pm for $SmSb_2O_4Cl$ and a = 783.56(4) pm, c = 1764.05(12) pm for $EuSb_2O_4Cl$ with Z = 8. Both can also be described with the crystal-chemical formula $Ln_2[Sb_4O_8]Cl_2$ for Z = 4, since they comprise isolated $[Sb_4O_8]^{4-}$ rings. This structural motif has some very close similarities to the known series of non-centrosymmetric $LnSb_2O_4Cl$ representatives (Ln = Gd–Lu), crystallizing in the tetragonal space group $P4_12$. All lanthanoid(III) cations have eight oxygen atoms as nearest neighbors arranged as square prisms $[LnO_8]^{13-}$, which are connected to layers by four parallel edges according to $^2_\infty\{[LnO^e_{8/2}]^{5-}\}$ with fluorite-like topology. The Sb^{3+} cations together with three oxygen atoms each and their lone-pair of electrons form ψ^1-tetrahedra $[SbO_3]^{3-}$. Four of these $[SbO_3]^{3-}$ entities join to $^0_\infty\{[Sb_4O_8]^{4-}\}$ rings with four bridging and four terminal oxygen atoms. Both centrosymmetric representatives, in contrast to the series of non-centrosymmetric ones, have a doubled lattice parameter c and several more symmetry elements, which will be discussed in detail.

Introduction

With a compound postulated as $SmSb_2O_4Cl$[1] analogous to $SmBi_2O_4Cl$ and the isotypic $LnBi_2O_4X$ representatives (Ln = La, Pr, Nd, Sm–Lu, X = Cl–I)[2–4] crystallizing tetragonally in the space group *P4/mmm*, the first rare-earth metal(III) oxidoantimonate(III) chloride was presented in 2000. However, no further statements and not even lattice parameters were given for this compound and it was not until 20 years later that $Sm_{1.3}Sb_{1.7}O_4Cl$[5] was obtained during an attempt to synthesize $Sm_5Cl_3[SbO_3]_4$ in analogy to $La_5Cl_3[SbO_3]_4$.[6] A peculiarity occurred here that the original Bi^{3+} position of $SmBi_2O_4Cl$ was mixed occupied with antimony and samarium in $Sm_{1+x}Sb_{2-x}O_4Cl$ with x = 0.3, which is already reflected by the lattice parameters of $SmBi_2O_4Cl$ (a = 388.72(1) pm, c = 895.0(2) pm)[4] in contrast to "$SmSb_2O_4Cl$" (a = 392.23(3) pm, c = 892.43(7) pm).[1] With a difference of 16 pm for the ionic radii ($r_i(Bi^{3+})$ = 0.96 pm versus $r_i(Sb^{3+})$ = 0.80 pm, both for *C.N.* = 4),[7] the expected lattice parameters for real "$SmSb_2O_4Cl$" would have been much smaller, more like $a \approx 380$ pm and $c \approx 885$ pm. But still the $(Sb/Sm)^{3+}$ cations arrange with four oxygen atoms to a square ψ^1_a-pyramid $[(Sb/Sm)O_4]^{5-}$ and the stereochemically active lone-pair of electrons occupies the apical position for the Sb^{3+} case. These pyramids are linked via four corners to form infinite layers according to $^2_\infty\{[(Sb/Sm)O^v_{4/2}]^-\}$ (Figure 1) by vertex-connectivity with isotactically oriented lone pairs.

In the targeted synthesis of $LnSb_2O_4Br$ representatives with Ln = Eu–Dy[8,9] and YSb_2O_4Br,[10] crystals were also obtained, but without a mixed occupation of the antimony position with any lanthanoid. In contrast to the previously mentioned structure, each Sb^{3+} cation forms a ψ^1-tetrahedron $[SbO_3]^{3-}$ with three oxygen atoms and a stereochemically active lone-pair of electrons. These pyramidal units are linked via two of their corners to form a meandering chain $^1_\infty\{[SbO^v_{2/2}O^t_{1/1}]^-\}$ (v = vertex-connecting, t = terminal). The tetragonal high-temperature structure of the $LnBi_2O_4X$ style is still visible via secondary contacts between the terminal oxygen atoms and the next to these atoms unbonded Sb^{3+} cations (Figure 2).

As in the case of the $LnSb_2O_4Br$ representatives and YSb_2O_4Br, Sb^{3+} again forms ψ^1-tetrahedra $[SbO_3]^{3-}$ with oxygen atoms in the analogous chloride representatives $LnSb_2O_4Cl$ (Ln = Gd–Lu)[11] and YSb_2O_4Cl,[10] but here four of these units form a closed eight-membered ring $^0_\infty\{[SbO^v_{2/2}O^t_{1/1}]^-)_4\}$ (v = vertex-connecting, t = terminal; Figure 3) via corner-linkage. In this structure, too, there are secondary contacts between all terminal oxygen atoms and the adjacent unbonded Sb^{3+} cations.

Regarding the lanthanoid-oxygen partial structure, which consists of fluorite-related layers $^2_\infty\{[LnO^e_{8/2}]^{5-}\}$ of $[LnO_8]^{13-}$ cubes sharing four parallel edges, one can find analogies to

[a] R. J. C. Locke, Prof. Dr. Th. Schleid
University of Stuttgart
Institute for Inorganic Chemistry
Pfaffenwaldring 55, 70569 Stuttgart
E-mail: ralf.locke@iac.uni-stuttgart.de
thomas.schleid@iac.uni-stuttgart.de

Supporting information for this article is available on the WWW under https://doi.org/10.1002/zaac.202200118

Journal of Inorganic and General Chemistry
ZAAC
Zeitschrift für anorganische und allgemeine Chemie

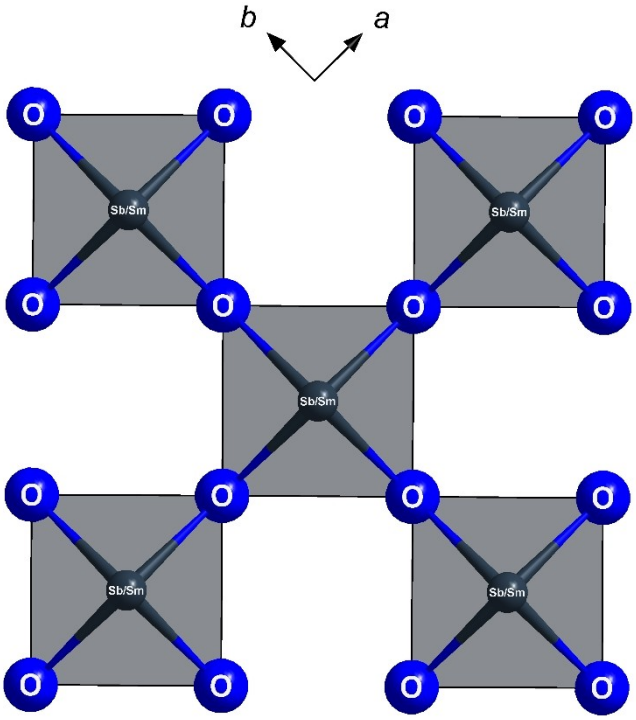

Figure 1. Layers $^{2}_{\infty}\{[(Sb/Sm)O^{v}_{4/2}]^{-}\}$ of vertex-linked square ψ^{1}_{a}-pyramids $[(Sb/Sm)O_4]^{5-}$ in the $SmBi_2O_4Cl$-related tetragonal crystal structure of $Sm_{1.3}Sb_{1.7}O_4Cl$.

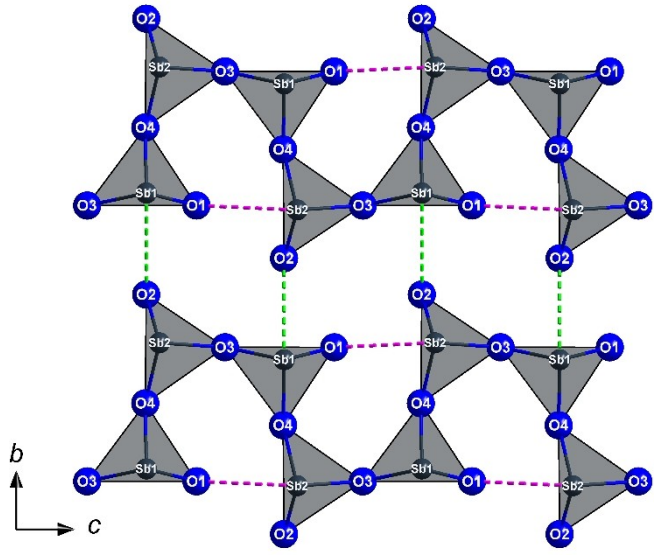

Figure 2. Meandering chains $^{1}_{\infty}\{[SbO^{v}_{2/2}O^{t}_{1/1}]^{-}\}$ of vertex-linked ψ^{1}-tetrahedra $[SbO_3]^{3-}$ in the monoclinic crystal structure of the $LnSb_2O_4Br$ representatives (Ln = Eu–Dy) and YSb_2O_4Br, which run parallel to the [001] direction. The secondary contacts of the terminal oxygen atoms to the next, not directly bonded Sb^{3+} cations are shown in pink within the chains and in green between the chains covering the (100) plane.

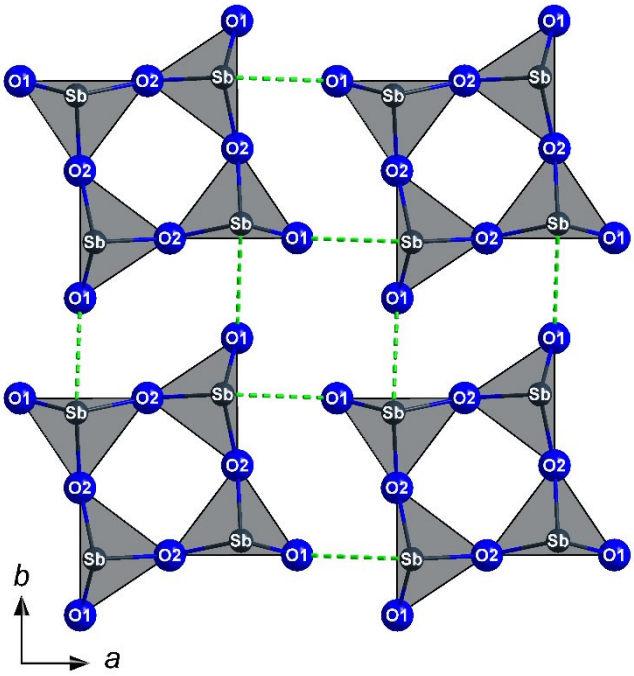

Figure 3. Isolated rings $[Sb_4O_8]^{4-}$ ($\equiv^{0}_{\infty}([SbO^{v}_{2/2}O^{t}_{1/1}]^{-})_4$ units) of four cyclically vertex-linked ψ^{1}-tetrahedra $[SbO_3]^{3-}$ in the tetragonal crystal structures of the $LnSb_2O_4Cl$ representatives (Ln = Sm and Eu; Gd–Lu) and YSb_2O_4Cl. The secondary contacts of the terminal oxygen atoms to the next, not directly bonded Sb^{3+} cations within the (001) plane are shown in green.

oxidotellurates(IV) with the composition $Na_2Ln_3Cl_3[TeO_3]_4$.[12–14] Occuring in both cases, they are sandwiched with lone-pair cations (Sb^{3+} or Te^{4+}) by capping the empty cubes under formation of $[SbO_3]^{3-}$ or $[TeO_3]^{2-}$ pyramids according to either $^{2}_{\infty}\{[Sb(LnO_{8/2})Sb]^{+}\}$ or $^{2}_{\infty}\{[Te_{2/3}(LnO_{8/2})Te_{2/3}]^{0.333+}\}$. These need to condense by sharing two vertices in the half-metal richer antimony(III) case, but remain isolated in the half-metal poorer tellurium(IV) case. With a single positive charge for the Sb^{3+}-containing ones, only parallel monolayers of Cl^{-} anions are necessary for charge compensation according to $LnSb_2O_4Cl$. The Te^{4+}-containing ones need extra Na^{+} cations alongside with monolayers of Cl^{-} anions to reach their electroneutrality according to $LnTe_{4/3}O_4ClNa_{2/3}$. In both cases, the lone pairs at the Sb^{3+} or Te^{4+} cations serve as inorganic antenna for the uptake of UV-radiation energy and its transfer to the Ln^{3+} cations within the fluorite-related layers $^{2}_{\infty}\{[LnO^{e}_{8/2}]^{5-}\}$ without any quenching Ln···Cl contacts. Suitable Ln^{3+} activator cations become excited and release their typical $4f$–$4f$ line emissions as luminescence. This mechanism has been proven for $YSb_2O_4Cl{:}Ln^{3+}$ and $Na_2Y_3Cl_3[TeO_3]_4{:}Ln^{3+}$ already with the yttrium compounds[10,12] as indifferent host materials and Ln = Eu, Tb[10] and others as luminophorous activators. So this article serves for a report on the true structure of $SmSb_2O_4Cl$ with discrete $[Sb_4O_8]^{4-}$ rings according to $Sm_2[Sb_4O_8]Cl_2$ on the one hand, but also as extension of our work on lone-pair assisted luminescence in layer-type compounds with fluorite-type $^{2}_{\infty}\{[LnO^{e}_{8/2}]^{5-}\}$ topology on the other.

By syntheses on target (see Experimental Section), the two new compounds $LnSb_2O_4Cl$ (Ln = Sm and Eu) were to be

Table 1. Crystallographic data for $SmSb_2O_4Cl$ and $EuSb_2O_4Cl$ as well as their determination.

	$SmSb_2O_4Cl$	$EuSb_2O_4Cl$
Crystal system	tetragonal	
Space group	*P*4 / *ncc* (no. 130)	
Lattice constants, *a* / pm	787.13(4)	783.56(4)
c / pm	1765.24(12)	1764.05(12)
c / *a*	2.243	2.251
Formula units, *Z*	8	
X-ray density, D_x / g·cm^{-3}	5.99	6.07
Molar volume, V_m / cm^3·mol^{-1}	82.33	81.54
Diffractometer	STADI-VARI (Stoe & Cie)	
Wavelength, λ / pm	71.07	
F(000)	1704	1712
Θ_{max} / °	33.06	32.17
hkl range ($\pm h_{max}$, $\pm k_{max}$, $\pm l_{max}$)	12, 12, 26	11, 11, 26
Unique reflections	1015	947
Absorption coefficient, μ / mm^{-1}	20.8	21.8
Absorption correction	Program X-SHAPE 2.21[25]	
R_{int} / R_σ	0.085 / 0.039	0.069 / 0.019
R_1 / R_1 with $\lvert F_o \rvert \geq 4\sigma(F_o)$	0.077 / 0.052	0.049 / 0.042
wR_2 / GooF	0.134 / 1.061	0.087 / 1.233
Structure determination and refinement	Program SHELX-97[26,27]	
Extinction coefficient, ε / 10^{-6} pm^{-3}	0.0005(1)	0.00125(6)
$\rho_{max/min}$ / e$^-$ 10^{-6} pm^{-3}	3.59 / −2.67	3.29 / −4.52
CSD number	2156776	2156779

produced and, especially in the case of the samarium representative, it was found out that this one also exists without stoichiometric problems and mixed cationic occupation in its crystal structure. So a particular focus needed to be put on the linkage of the Sb^{3+} cations and their coordination polyhedra.

Results and Discussion

The two new compounds $SmSb_2O_4Cl$ and $EuSb_2O_4Cl$ both crystallize in the tetragonal space group *P*4/*ncc* (origin choice 2, origin at $\bar{1}$ ($^1/_4$, $-^1/_4$, 0 from $\bar{4}$)) with the lattice parameters a = 787.13(4) pm and c = 1765.24(12) pm for the samarium and a = 783.56(4) pm and c = 1764.05(12) pm for the europium representative, both with Z = 8 (Table 1). They can also be described with the structured molecular formula $Ln_2[Sb_4O_8]Cl_2$ (*Ln* = Sm and Eu) for Z = 4, since they comprise eight-membered $[Sb_4O_8]^{4-}$ rings with four bridging and four terminal oxygen atoms of the envolved ψ^1-tetrahedral $[SbO_3]^{3-}$ units according to $^0_\infty\{[SbO^v_{2/2}O^t_{1/1}]^-)_4\}$. There is only one unique antimony (16 *g*, Table 2), but two crystallographically distinct lanthanoid cations (4*a* and 4*c*) in the crystal structure, which do not show any mixed occupancy. Even for the oxygen atoms there are two distinct crystallographic sites (16 *g* for both) and the same is true for chlorine (4*b* and 4*c*, Table 2).

Figure 4 shows the oxygen atoms coordination spheres for the two crystallographically different Ln^{3+} cations. They are each surrounded by eight oxygen atoms arranged as square prisms $[LnO_8]^{13-}$ and linked by four of their edges according to $^2_\infty\{[LnO^e_{8/2}]^{5-}\}$ (*e* = edge-connected) to form fluorite-like layers parallel to the (001) plane. The detailed Ln^{3+}–O^{2-} distances of 230–262 pm for *C.N.* = 8 can be found in Table 3 and agree quite well in comparison with those of the respective Ln_2O_3 representatives in the monoclinic B- or Sm_2O_3-type structures

Table 2. Atomic coordinates, *Wyckoff* positions and equivalent isotropic displacement parameters for $SmSb_2O_4Cl$ (*top*) and $EuSb_2O_4Cl$ (*bottom*).

Atom	Site	*x*/*a*	*y*/*b*	*z*/*c*	U_{eq} / pm^2[b]
Sm1	4*a*	$^3/_4$	$^1/_4$	$^1/_4$	111(3)
Sm2	4*c*	$^1/_4$	$^1/_4$	0.26044(6)	116(3)
Sb[a]	16*g*	0.05542(19)	0.99245(19)	0.10525(5)	110(4)
O1	16*g*	0.0022(12)	0.8236(12)	0.1821(5)	235(18)
O2	16*g*	0.0035(12)	0.2151(12)	0.1623(5)	200(17)
Cl1	4*b*	$^3/_4$	$^1/_4$	0	248(12)
Cl2	4*c*	$^1/_4$	$^1/_4$	0.4916(4)	269(13)
Sb′[a]	*16g*	*0.9926(15)*	*0.0557(15)*	*0.1057(3)*	*200(24)*
Eu1	4*a*	$^3/_4$	$^1/_4$	$^1/_4$	87(3)
Eu2	4*c*	$^1/_4$	$^1/_4$	0.25982(6)	90(3)
Sb[a]	16*g*	0.05392(16)	0.99206(16)	0.10556(4)	85(3)
O1	16*g*	0.0026(11)	0.8199(11)	0.1813(4)	158(16)
O2	16*g*	0.0037(11)	0.2134(11)	0.1631(4)	132(15)
Cl1	4*b*	$^3/_4$	$^1/_4$	0	209(11)
Cl2	4*c*	$^1/_4$	$^1/_4$	0.4921(4)	248(12)
Sb′[a]	*16g*	*0.988(3)*	*0.054(3)*	*0.1056(9)*	*80(8)*

[a] partial occupation of Sb with *Sb′* exhibiting site occupation factors *s.o.f.*(Sb) = 0.84(1) for *Ln* = Sm and *s.o.f.*(Sb) = 0.92(1) for *Ln* = Eu, adding up to 1.00 with *s.o.f.*(*Sb′*) = 0.16(1) for *Ln* = Sm and *s.o.f.*(*Sb′*) = 0.08(1) for *Ln* = Eu as refinement constraint PART in the SHELX suite.[26,27] [b] The anisotropic displacement parameters are listed in Table S1 for $SmSb_2O_4Cl$ and Table S2 for $EuSb_2O_4Cl$ in the Supplementary Information.

Journal of Inorganic and General Chemistry
ZAAC
Zeitschrift für anorganische und allgemeine Chemie

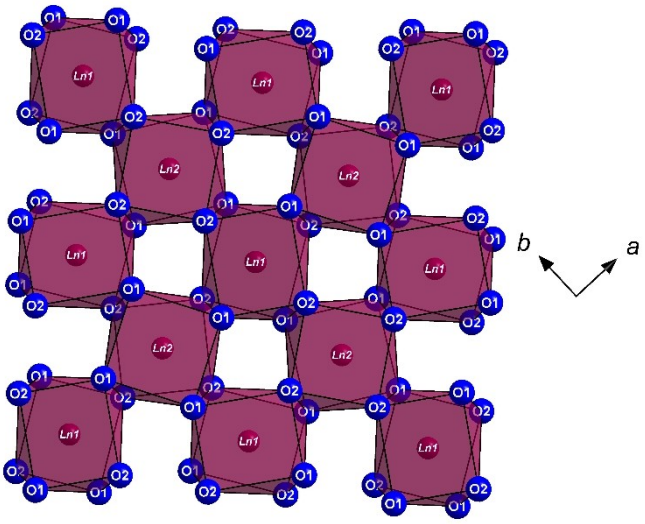

Figure 4. Infinite layer $^{2}_{\infty}\{[LnO^{e}_{8/2}]^{5-}\}$ of edge-linked square $[LnO_8]^{13-}$ prisms parallel to the (001) plane in the tetragonal crystal structure of the $LnSb_2O_4Cl$ representatives (Ln = Sm and Eu).

Table 3. Selected interatomic distances (d / pm) for $SmSb_2O_4Cl$ (*left*) and $EuSb_2O_4Cl$ (*right*).

$SmSb_2O_4Cl$		distance	$EuSb_2O_4Cl$		distance
Sm1–O1	(4×)	236.1(9)	Eu1–O1	(4×)	235.1(9)
Sm1–O2	(4×)	254.1(9)	Eu1–O2	(4×)	252.6(8)
Sm2–O1	(4×)	230.3(9)	Eu2–O1	(4×)	230.1(9)
Sm2–O2	(4×)	261.6(9)	Eu2–O2	(4×)	259.1(8)
Sb–O1	(1×)	194.5(9)	Sb–O1	(1×)	194.1(8)
Sb–O2	(1×)	206.2(9)	Sb–O2	(1×)	204.8(8)
Sb–O2′	(1×)	207.0(9)	Sb–O2′	(1×)	208.9(8)
Sb···O1′	(1×)	327.8(9)	Sb···O1′	(1×)	322.1(8)
Sm1···Cl1	(2×)	441.3(8)	Eu1···Cl1	(2×)	441.0(7)
Sm2···Cl2	(1×)	408.1(8)	Eu2···Cl2	(1×)	409.8(7)
Sb···Cl1	(1×)	307.24(13)	Sb···Cl1	(1×)	307.01(11)
Sb···Cl1′	(1×)	365.25(14)	Sb···Cl1′	(1×)	363.64(11)
Sb···Cl2	(1×)	323.7(5)	Sb···Cl2	(1×)	323.3(5)
Sb···Cl2′	(1×)	351.3(4)	Sb···Cl2′	(1×)	349.8(4)

spanning intervals from 235 to 254 pm for *C.N.* = 6 and 7[15,16] as typical ranges for these element combinations. This structural arrangement for mid-size Ln^{3+} cations mediates between the trigonal A-type[17,18] and the cubic C-type structure[19,20] of the lanthanoid sesquioxides Ln_2O_3 exhibiting coordination numbers of seven in the first and six in the second case.

From this point of view, $SmSb_2O_4Cl$ and $EuSb_2O_4Cl$ resemble a lot the architecture of the following members of the $LnSb_2O_4Cl$ series with Ln = Gd–Lu.[11] Even the ψ^1-tetrahedral $[SbO_3]^{3-}$ units with d(Sb–O) = 194–195 pm for the terminal and 205–209 for the bridging ones as well as their vertex-connectivity among four of them to form discrete eight-membered $[Sb_4O_8]^{4-}$ rings according to $^{0}_{\infty}\{[SbO^{v}_{2/2}O^{t}_{1/1}]^{-})_4\}$ are very much alike. The main difference arises from the centrosymmetric space group $P4/ncc$ for $SmSb_2O_4Cl$ and $EuSb_2O_4Cl$ versus $P42_12$ for the non-centrosymmetrically crystallizing congeners (Ln = Gd–Lu) in combination with an approximately doubled lattice parameter c. With halved values for their lattice parameter c ($c/2 \approx 882.6$ pm for Ln = Sm, $c/2 \approx 882.0$ pm for Ln = Eu) and c/a ratios ($c/2a = 1.121$ for Ln = Sm, $c/2a = 1.126$ for Ln = Eu), they would even perfectly continue the trend of Table 4 towards the lighter lanthanoids. The $[Sb_4O_8]^{4-}$ rings at the heights $z/c \approx {}^{1}/_{8}$ (rotation anti-clockwise) and $z/c \approx {}^{3}/_{8}$ (rotation clockwise), respectively, called layer 1 in the following, can be transferred by inversion symmetry into those at the heights $z/c \approx {}^{7}/_{8}$ (rotation anti-clockwise) and $z/c \approx {}^{5}/_{8}$ (rotation clockwise), respectively, dubbed as layer 2 (Figure 5). The bridging oxygen atoms exhibit distances from 205 to 209 pm (Table 3) to the Sb^{3+} cations, whereas the terminal ones show much shorter values (194–195 pm, Table 3). These distances represent quite typical antimony(III)-oxygen distances, when compared with those in senarmontite[21] (α-Sb_2O_3: d(Sb–O) = 198 pm, 3×) with discrete Sb_4O_6-cage molecules or in

Table 4. Lattice parameters and molar volumes (V_m /$cm^3 \cdot mol^{-1}$) of all tetragonal $LnSb_2O_4Cl$ representatives with Ln = Sm–Lu and YSb_2O_4Cl.

Ln	a / pm	c / pm	c / a	V_m	Lit.
Sm[a]	787.13(4)	1765.24(12)	2.243 (2×1.121)	82.33	
Eu[a]	783.56(4)	1764.06(12)	2.251 (2×1.126)	81.54	
Gd[b]	781.08(4)	881.47(6)	1.129	80.97	[11]
Tb[b]	778.53(4)	880.92(6)	1.132	80.39	[11]
Dy[b]	776.17(4)	880.34(6)	1.134	79.85	[11]
Ho[b]	773.64(4)	879.53(6)	1.137	79.25	[11]
Y[b]	773.56(4)	878.91(6)	1.136	79.19	[10]
Er[b]	771.35(4)	879.16(6)	1.140	78.67	[11]
Tm[b]	769.03(4)	878.62(6)	1.143	78.08	[11]
Yb[b]	766.72(4)	878.05(6)	1.145	77.65	[11]
Lu[b]	764.59(4)	877.48(6)	1.148	77.25	[11]

[a] space group: $P4/ncc$ (no. 130); [b] space group: $P42_12$ (no. 90).

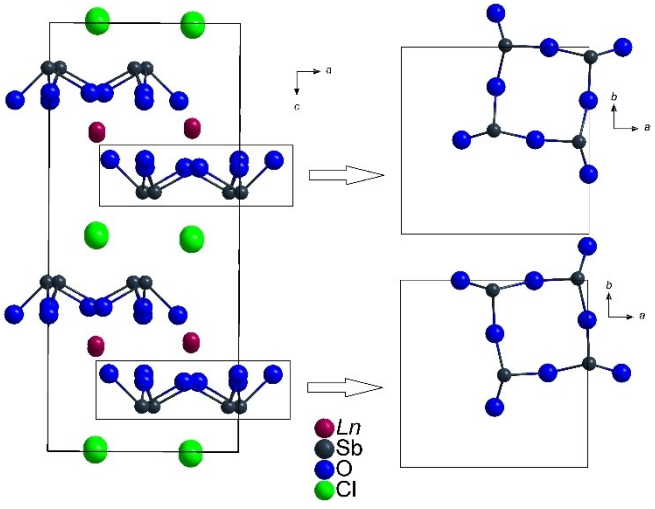

Figure 5. Unit cell of the $LnSb_2O_4Cl$ representatives (Ln = Sm and Eu) in the tetragonal space group $P4/ncc$ as viewed along [010] (*left*), showing non-conformal $[Sb_4O_8]^{4-}$ rings at the $z/c \approx {}^{1}/_{8}$ (*bottom*) and the $z/c \approx {}^{5}/_{8}$ (*top*) level as (001) projections (*right*).

valentinite[22] (β-Sb_2O_3: d(Sb–O) = 198–202 pm *plus* 252 and 262 pm), for example. The O–Sb–O angles of 83–102° and the 116-pm deflection of the Sb^{3+} cations from their (O1,O2,O2′) plane attests for more p-character in the Sb–O bonds and more s-character of their lone pairs than expected for an ideal sp^3-hybridization.

The Cl^- anions show a minimum distance of 307 pm to the next Sb^{3+} cation and to the next Ln^{3+} cation it amounts to even 408 pm. With such large separations, it can probably no longer be assumed that there is a real coordination effect. Figure 5 presents an almost complete unit cell of the tetragonal $LnSb_2O_4Cl$ representatives in the space group *P4/ncc* as viewed along [100]. Between the layers of Sb^{3+} cations reside the layers of Cl^- anions with almost no connectivity. Thus, these are not really closely connected to another layer, because two layers of Sb^{3+} cations flank the layers of Ln^{3+} cations via the oxygen atoms according to $^{2}_{\infty}\{[Sb(LnO^{e}_{8/2})Sb]^+\}$. The Cl^- anion layers serve to compensate the charge the $[Sb(LnO_4)Sb]^+$ layers, so without these, no stability for the whole crystal structure would be expected and this fact has again resemblance to the rest of the $LnSb_2O_4Cl$ series with Ln = Gd–Lu[11] and YSb_2O_4Cl,[10] all crystallizing in the non-centrosymmetric space group $P42_12$ (Table 4). The distances of the Sb^{3+} cations to the nearest, but not directly bonded, terminal oxygen atoms (O1′) of adjacent rings (dotted green connections in Figure 3) amount to d(Sb–O1′) = 322 pm for $EuSb_2O_4Cl$ and d(Sb–O1′) = 328 pm for $SmSb_2O_4Cl$. Although they appear rather long in comparison to the covalently bonded ones (d(Sb–O) = 194–209 pm, Table 3), they clearly show that Sb^{3+} strives for a fourfold coordination, as it is already known for the $LnBi_2O_4X$ representatives (Ln = La–Lu, X = Cl–I)[2–4] and $Sm_{1+x}Sb_{2-x}O_4X$ (X = Cl and Br),[5] which might be due to the fact that there is a high-temperature phase present at the reaction temperatures, most likely crystallizing analogously to the *P4/mmm*-type $LnBi_2O_4X$ representatives (Figure 6, *top*), if necessary stabilized by some Ln^{3+} surplus.[5]

A link between the quadruple and triple oxygen-atom coordination of antimony(III) is not yet known so far, but a new monoclinic modification of $LaBi_2O_4Cl$[24] exhibits an infinite strand from fused components of this mixed coordination (Figure 7). The square ψ^1_a-pyramids $[BiO_4]^{5-}$ form a meandering chain via *cis*-oriented oxygen atoms by corner-linkage according to $^{1}_{\infty}\{[BiO^{v}_{2/2}O^{t}_{2/1}]^{3-}\}$. In this process, the terminal oxygen atoms of this chain are linked to ψ^1-tetrahedra $[BiO_3]^{3-}$. This results in a ribbon (Figure 7), where the terminal oxygen atoms (O4) are not linked to the next but one bismuth(III) cations with secondary contacts any more.

In order to prove the phase purity of the $SmSb_2O_4Cl$ sample, a powder X-ray diffractogram was recorded, which is shown in Figure 8.

For further characterization, on $SmSb_2O_4Cl$ a single-crystal Raman measurement was performed with an excitation wavelength of λ = 638 nm and the recorded spectrum is shown in Figure 9. The strongest band at $\tilde{\nu}$ = 702 cm^{-1} can be attributed to the valence vibration of the oxygen atoms terminally bound to antimony ν(Sb–O_t) in common mode, while the very small band at $\tilde{\nu}$ = 672 cm^{-1} originates from the push-pull vibration. The band appearing at $\tilde{\nu}$ = 562 cm^{-1} also belongs to a valence

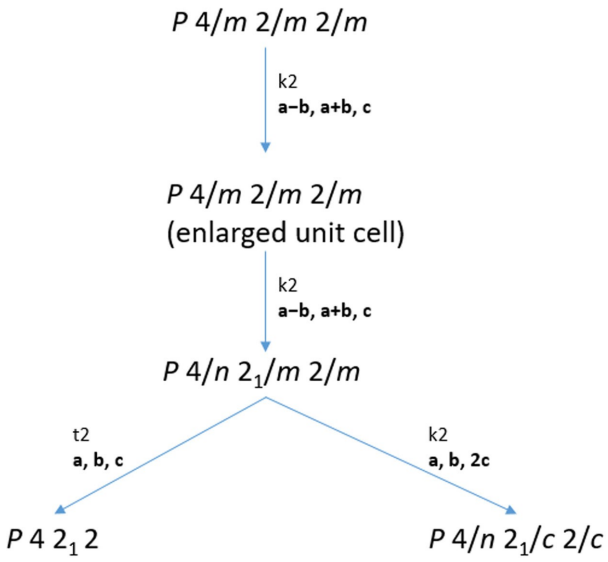

Figure 6. Condensed Bärnighausen symmetry tree for the group-subgroup relationship between the HT- and LT-modifications of the $LnSb_2O_4Cl$ series with Ln = Sm–Lu.

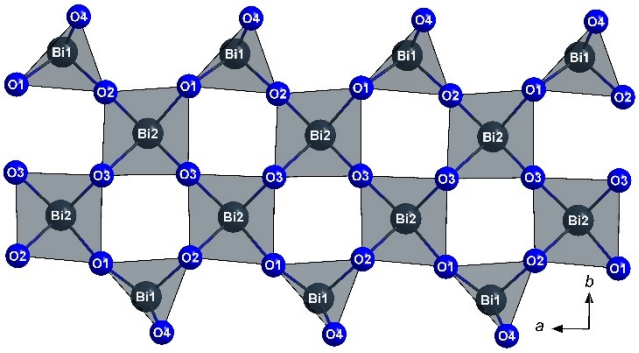

Figure 7. Oxygen-atom coordination of bismuth(III) in a new monoclinic modification of $LaBi_2O_4Cl$ with triple and quadruple coordination of Bi^{3+} by oxygen.[24]

vibration, but in this case to the common mode vibration of the samarium-oxygen prisms $\nu(SmO_8)$. The region with bands at $\tilde{\nu}$ = 464, 405, 357 and 314 cm^{-1} derives from the valence vibrations $\nu(Sb_4O_4)$ of the bridging oxygen atoms within the $[Sb_4O_8]^{4-}$ ring. Finally, the front region with its five strong bands at $\tilde{\nu}$ = 217, 178, 147, 131, 113 and 97 cm^{-1} has to be assigned to the deformation vibrations $\delta(Sb_4O_4)$ and $\delta(SmO_8)$.[28,29] The measurement shows a great similarity with the Raman spectrum of $GdSb_2O_4Cl$.[11] This does not come unexpected, since the structural features of these two different structures are roughly the same. A Raman spectrum of $EuSb_2O_4Cl$ could not be recorded due to Eu^{3+}-luminescence phenomena. Unfortunately, pure $EuSb_2O_4Cl$ is not showing any bulk luminescence due to concentration quenching, however, but Eu^{3+}-doped samples of YSb_2O_4Cl[10] and $GdSb_2O_4Cl$[23] do.

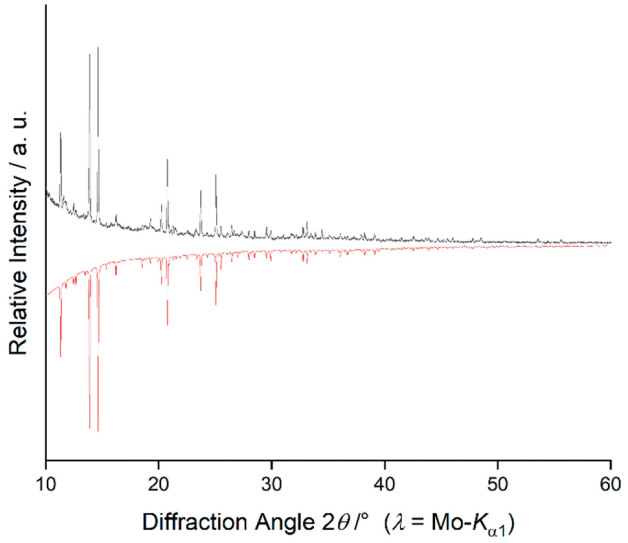

Figure 8. Powder X-ray diffractogram of $SmSb_2O_4Cl$.

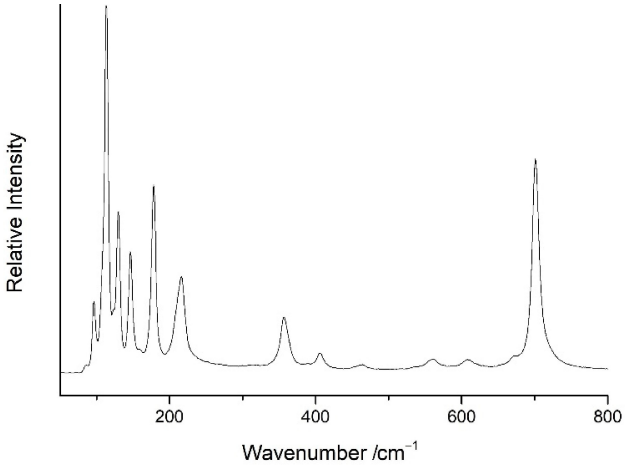

Figure 9. Single-crystal Raman spectrum of $SmSb_2O_4Cl$.

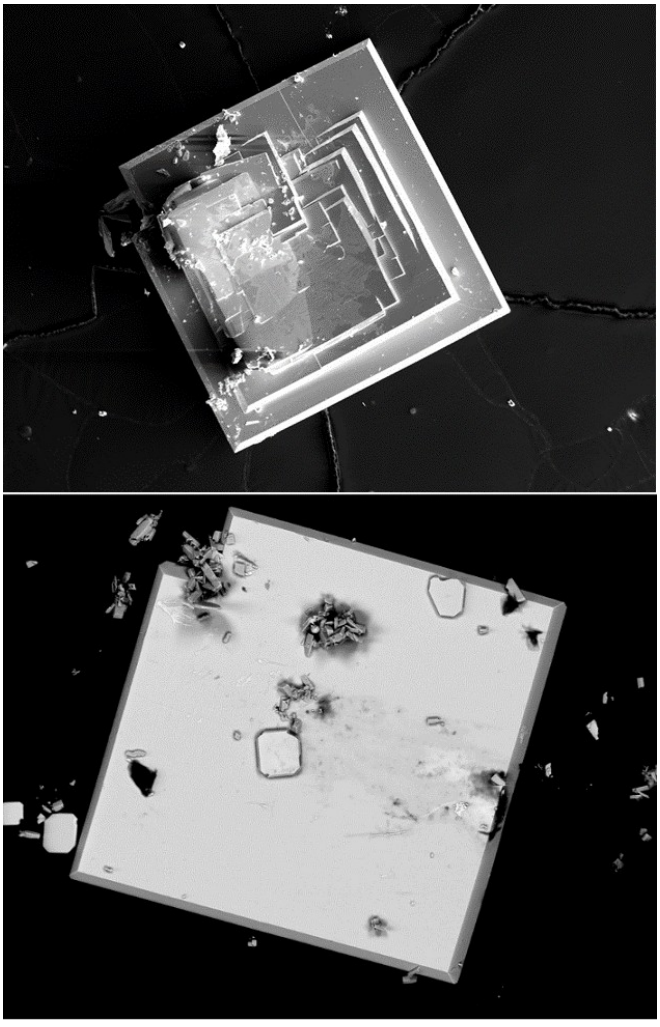

Figure 10. Scanning electron micrographs (SEM) of the platelet-shaped crystals of $SmSb_2O_4Cl$ (*top*) and $EuSb_2O_4Cl$ (*bottom*).

SEM images of $SmSb_2O_4Cl$ and $EuSb_2O_4Cl$ (Figure 10) were acquired using an electron-beam microprobe (SX-100, Cameca). Both crystals have edge lengths of approximated one millimeter.

In order to verify the exact composition of the individual compounds, an EDXS measurement based on energy dispersive X-ray spectroscopy was carried out for the example of $EuSb_2O_4Cl$ using the electron-beam microprobe. According to Figure 11, only the four elements europium at 12.8(2)% (ideal: 12.5%), antimony at 25.8(2)% (ideal: 25.0%), oxygen at 50.6(3)% (ideal: 50.0%) and chlorine at 12.7(4)% (ideal: 12.5%) are visible. The ratio of europium to antimony equals 1:2, which means that there is no mixed occupation in this compound as in the case of $Sm_{1.3}Sb_{1.7}O_4Cl$,[5] for example. WDXS measurements were performed for $SmSb_2O_4Cl$ as well and the following results emerged: samarium 11.9(5)% (ideal: 12.5%), antimony 25.5(3)% (ideal: 25.0%), oxygen 50.5(4)% (ideal: 50.0%),

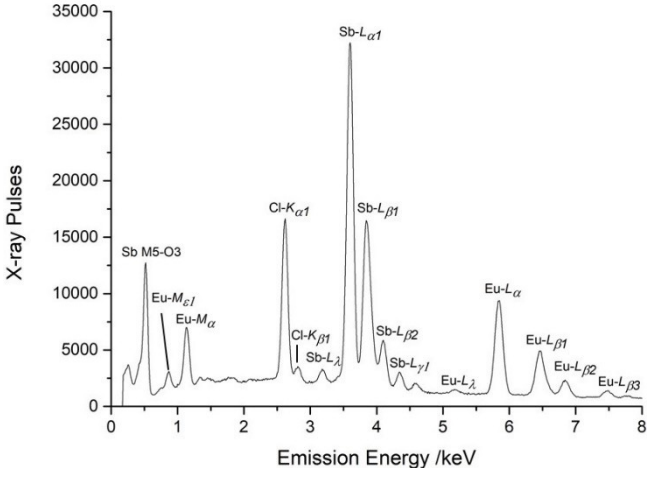

Figure 11. EDXS measurement on a single crystal of $EuSb_2O_4Cl$ with an accelerating voltage of $U = 20$ keV.

chlorine 12.1(4)% (ideal: 12.5%). So all studies confirmed the empirical formulae $SmSb_2O_4Cl$ and $EuSb_2O_4Cl$.

Conclusions

The two new lanthanoid(III) oxidoantimonate(III) chlorides $SmSb_2O_4Cl$ and $EuSb_2O_4Cl$ were obtained via solid-state reactions. Both crystallize tetragonally in the centrosymmetric space group *P4/ncc* with the lattice parameters $a = 787.13(4)$ pm, $c = 1765.24(12)$ pm for $SmSb_2O_4Cl$ and $a = 783.56(4)$ pm, $c = 1764.05(12)$ pm for $EuSb_2O_4Cl$ with $Z = 8$. As compared to the tetragonal non-centrosymmetric $LnSb_2O_4Cl$ representatives with Ln = Gd–Lu and YSb_2O_4Cl in the space group $P42_12$, a doubling of the lattice parameter *c* occurs. Both structure types show no mixed occupation in contrast to the previously investigated $Sm_{1+x}Sb_{2-x}O_4Cl$, which could also be demonstrated explicitly with electron-beam microprobe measurements. However, the centrosymmetric structures show some stacking faults, which are most probably due to a high-temperature phase with $SmBi_2O_4Cl$ topology. If the lattice parameter *c* of $SmSb_2O_4Cl$ is theoretically bisected, a cell with $a \approx 787$ pm and $c/2 \approx 883$ pm emerges, which perfectly matches with the $P42_12$ representatives. If the lattice parameter *a* is now also bisected, a cell with $a/2 \approx 394$ pm and $c/2 \approx 883$ pm results, which almost equals the one of $Sm_{1+x}Sb_{2-x}O_4Cl$ ($a = 392.24(3)$ pm and $c = 892.43(7)$ pm). The significant deviation by nearly 10 pm of the lattice parameter *c* comes from the mixed occupation of the antimony position with samarium. This suggests that the high-temperature phase can be stabilized by an excess of Ln^{3+} cations. But even without, a unit cell like $a \approx 393.6$ pm and $c \approx 882.6$ pm should occur for the room-temperature quenched high-temperature phase of $SmSb_2O_4Cl$ in space group *P4/mmm*. Despite *P4/ncc* (≡ *P* 4/*n* 2$_1$/*c* 2/*c*, no. 130) is a minimal non-isomorphic supergroup of $P42_12$ (*P* 4 2$_1$ 2, no. 90), the crystal structures of $EuSb_2O_4Cl$ and $GdSb_2O_4Cl$ can not be easily transferred into each other by just halving or doubling the lattice parameter *c* (Figure 6). In the crystal structure of the $GdSb_2O_4Cl$ type, all $\{(Ln[Sb_4O_8]Ln)^+\}$ layers are identical by translation symmetry, but in the $EuSb_2O_4Cl$-type structure, there is an AB stacking that causes a larger unit cell and a change in the space-group symmetry. The reason for their differentiation is not yet clear, since neither the space fillings as calculated with the MAPLE program using the *Shannon* ionic radii $r_i(O^{2-}) = 140$ pm for *C.N.* = 6, $r_i(Cl^-) = 181$ pm for *C.N.* = 6, $r_i(Sb^{3+}) = 76$ pm for *C.N.* = 3, $r_i(Eu^{3+}) = 107$ pm for *C.N.* = 8 and $r_i(Gd^{3+}) = 105$ pm for *C.N.* = 8 of 73.7% for $EuSb_2O_4Cl$ and 73.9% for $GdSb_2O_4Cl$ differ much, nor the MAPLE values (21,169 kJ/mol for $EuSb_2O_4Cl$ versus 21,225 kJ/mol for $GdSb_2O_4Cl$) themselves. Moreover, the symmetry densities with about 40 for the number of refined parameters are almost identical. The formation of these different structures can not result from different synthesis conditions, since they were all synthesized together at the same time in the same furnace. Future investigations need to show, whether one can provoke a temperature-induced phase transition from one into the other structure and if there is a common tetragonal high-temperature phase in the space group *P4/mmm* (≡ *P* 4/*m* 2/*m* 2/*m*, no. 123) according to the aristotypic lanthanoid(III) oxidobismuthate(III) chlorides $LnBi_2O_4Cl$ (Ln = La–Lu).

Experimental Section

Product Synthesis

The corresponding lanthanoid sesquioxides (Ln_2O_3, ChemPur: 99.99% for Ln = Sm and Eu) were reacted with the lanthanoid trichlorides ($LnCl_3$, ChemPur: 99.9% for Ln = Sm; Aldrich: 99.99% for Ln = Eu) and antimony sesquioxide (Sb_2O_3, ChemPur: 99.9%) via solid-state reactions to yield the lanthanoid(III) oxidoantimonate(III) chlorides $LnSb_2O_4Cl$ (Equation 1). In all cases, eutectic mixtures of cesium chloride (CsCl, Aldrich: 99.9%) and sodium chloride (NaCl, Merck: 99.99%) were chosen as flux. The reactions always took place in evacuated glassy silica ampoules according to:

$$Ln_2O_3 + LnCl_3 + 3\ Sb_2O_3 \xrightarrow{\text{flux}} 3\ LnSb_2O_4Cl \quad (1)$$

$$(\text{flux}:\ CsCl + NaCl,\ Ln = \text{Sm and Eu}).$$

The reactants were weighed into glassy silica ampoules under inert gas (argon) in a glove box (Glovebox Systemtechnik, GS Mega E-line), sealed under dynamic vacuum and reacted in a muffle furnace (Nabertherm, L9/12) at a specific temperature program. This involved heating to 750 °C at a heating rate of 150 °C/h and holding at this temperature for two days. Cooling at 5 °C/h brought the vials down to 666 °C and again this temperature was held for two days. Renewed cooling at 5 °C/h took the ampoules to 530 °C and afterwards this temperature was maintained again for two days. In the final step, cooling at 10 °C/h to 480 °C and eventually at 150 °C/h to room temperature took place. These three temperature plateaus were chosen to allow as much crystal growth as possible. In addition, slow cooling rates were applied to avoid exposing the crystals to thermal stress. The reaction products were then washed with 500 ml of demineralized water and dried at 120 °C in a drying oven. Under the stereomicroscope, almost colorless, flat, platelet-shaped crystals were found in all cases, showing the very pale color of the involved Ln^{3+} cation (Sm^{3+}: yellow, Eu^{3+}: white).

Single-Crystal X-Ray Diffraction

Suitable crystals were selected from the samples and fixed in glass capillaries (Hilgenberg, Malsfeld; outer diameter: 0.1 mm, wall thickness: 0.01 mm) with grease. Measurements were carried out with a single-crystal diffractometer (STADI-VARI, STOE, Darmstadt, Germany). The tetragonal crystal structure of both $LnSb_2O_4Cl$ representatives with Ln = Sm (CSD number: 2156776) and Ln = Eu (CSD number: 2156779) was solved using direct methods in the centrosymmetric space group *P4/ncc* and refined with the SHELX-97 program package. The highest peaks in the final difference Fourier maps showed coordinates like $x/a \approx y/b$(Sb), $y/b \approx x/a$(Sb), $z/c \approx z/c$(Sb) in both cases, which are related to each other within the limits of error, indicating some disorder of the stacking sequence. A suitable interpretation for this phenomenon could be that the sequence "layer 1 ($[Sb_4O_8]^{4-}$ ring centered at $^1/_4$, $^1/_4$, $z/c \approx 0.1$, rotation anti-clockwise, ($[Sb_4O_8]^{4-}$ ring centered at $^3/_4$, $^3/_4$, $z/c \approx 0.4$) and layer 2 ($[Sb_4O_8]^{4-}$ ring centered at $^1/_4$, $^1/_4$, $z/c \approx 0.6$, rotation anti-clockwise, ($[Sb_4O_8]^{4-}$ ring centered at $^3/_4$, $^3/_4$, $z/c \approx 0.9$)" might be statistically inverted in every tenth layer. The crystallographic data without refinement of *Sb*' with the PART command can be found in Tables S3 and S4 of the Supplementary Information

and striking here are the very high residual electron densities close to the respective Sb position.

Powder X-Ray Diffraction

The powder X-ray diffraction pattern of $SmSb_2O_4Cl$ was recorded using a STADI-P diffractometer (Stoe & Cie, Darmstadt, Germany) with Ge(111)-monochromatized molybdenum radiation ($\lambda =$ 71.07 pm).

Raman Spectroscopy

A Raman spectrum for the single crystal of $SmSb_2O_4Cl$ was recorded using a Raman microscope (XploRA, Horiba, Kyoto) with an excitation wavelength of $\lambda = 638$ nm at a LASER power of 25 mW.

Electron-Beam Microprobe Analysis

The EDXS and WDXS measurements and the SEM images of $SmSb_2O_4Cl$ and $EuSb_2O_4Cl$ were acquired using an electron-beam X-ray microprobe (SX-100, Cameca, Gennevilliers).

Acknowledgements

We thank Dr. Falk Lissner (AOR, Univ. Stuttgart) for the single-crystal X-ray diffraction measurements, Dr. Felix C. Goerigk (Leuchtstoffwerk Breitungen GmbH) for the EDXS or WDXS measurements and M.Sc. Jean-Louis Hoslauer (Univ. Stuttgart) for the powder X-ray diffraction measurements. Open Access funding enabled and organized by Projekt DEAL.

Conflict of Interest

The authors declare no conflict of interest.

Data Availability Statement

The data that support the findings of this study are available in the supplementary material of this article.

Keywords: Lanthanoids · Oxidoantimonates(III) · Chlorides · Crystal Structure · Raman Spectrum

[1] M. Schmidt, H. Oppermann, M. Zhang-Preße, E. Gmelin, W. Schnelle, N. Söger, M. Binnewies, *Z. Anorg. Allg. Chem.* **2001**, *627*, 2105–2111.
[2] C. J. Milne, P. Lightfoot, J. D. Jorgensen, S. Short, *J. Mater. Chem.* **1995**, *5*, 1419–1421.
[3] M. Schmidt, H. Oppermann, *Z. Anorg. Allg. Chem.* **1999**, *625*, 544–546.
[4] M. Schmidt, H. Oppermann, C. Henning, R. W. Henn, E. Gmelin, N. Söger, *Z. Anorg. Allg. Chem.* **2000**, *626*, 125–135.
[5] F. C. Goerigk, Th. Schleid, *Z. Anorg. Allg. Chem.* **2019**, *645*, 1079–1084.
[6] F. C. Goerigk, *Doctoral Dissertation*, Univ. Stuttgart **2021**.
[7] R. D. Shannon, *Acta Crystallogr.* **1975**, *32*, 751–767.
[8] F. C. Goerigk, V. Paterlini, K. V. Dorn, A.-V. Mudring, Th. Schleid, *Crystals* **2020**, *10*, 1089–1112.
[9] R. J. C. Locke, F. C. Goerigk, Th. Schleid, *Z. Kristallogr.* **2021**, *S 41*, 78–79.
[10] R. J. C. Locke, F. C. Goerigk, M. J. Schäfer, H. A. Höppe, Th. Schleid, *Roy. Soc. Chem. Adv.* **2022**, *12*, 640–647.
[11] R. J. C. Locke, F. C. Goerigk, Th. Schleid, *Z. Naturforsch.* **2022**, *77b*, in print; https://doi.org/10.1515/znb-2022–0004.
[12] S. Zitzer, F. Schleifenbaum, Th. Schleid, *Z. Naturforsch.* **2014**, *69b*, 150–158.
[13] D. O. Charkin, S. Zitzer, S. Greiner, S. G. Dorofe′ev, A. V. Olenev, P. S. Berdonosov, Th. Schleid, V. A. Dolgikh, *Z. Anorg. Allg. Chem.* **2017**, *643*, 1654–1660.
[14] S. Greiner, S. Zitzer, S. Strobel, P. S. Berdonosov, Th. Schleid, *Z. Kristallogr.* **2020**, *235*, 341–352.
[15] Th. Schleid, G. Meyer, *J. Less-Common Met.* **1989**, *149*, 73–80.
[16] G. Chen, J. R. Peterson, K. E. Brister, *J. Solid State Chem.* **1994**, *111*, 437–439.
[17] W. H. Zachariasen, *Z. Phys. Chem.* **1926**, *123*, 134–150.
[18] H. Bärnighausen, G. Schiller, *J. Less-Common Met.* **1985**, *110*, 385–390.
[19] H. Bommer, *Z. Anorg. Allg. Chem.* **1939**, *241*, 273–280.
[20] G. Brauer, H. Gradinger, *Z. Anorg. Allg. Chem.* **1954**, *276*, 209–226.
[21] C. Svensson, *Acta Crystallogr.* **1975**, *31*, 2016–2018.
[22] B. Antic, P. Oennerud, D. Rodic, R. Tellgren, *Powder Diffr.* **1993**, *8*, 216–220.
[23] R. J. C. Locke, *Doctoral Dissertation*, Univ. Stuttgart, *in preparation*.
[24] A. Nakada, D. Kato, R. Nelson, H. Takahira, M. Yabuuchi, M. Higashi, H. Suzuki, M. Kirsanova, N. Kakudou, C. Tassel, T. Yamamoto, C. M. Brown, R. Dronskowski, A. Saeki, A. Abakumov, H. Kageyama, R. Abe, *J. Am. Chem. Soc.* **2021**, *143*, 2491–2499.
[25] W. Herrendorf, H. Bärnighausen, HABITUS: Program for the Optimisation of the Crystal Shape for Numerical Absorption Correction in X-SHAPE, Version 1.06, Stoe, Darmstadt **1999**, Karlsruhe **1993**, Gießen **1996**.
[26] G. M. Sheldrick, SHELXS-97 and SHELXL-97: Programs for the Solution and Refinement of Crystal Structures from X-Ray Diffraction Data, Göttingen **1997**.
[27] G. M. Sheldrick, *Acta Crystallogr.* **2008**, *A 64*, 112–122.
[28] J. Weidlein, U. Müller, K. Dehnicke, *Schwingungsfrequenzen I – Hauptgruppenelemente*, 1. Auflage, Georg-Thieme-Verlag, Stuttgart, New York **1981**.
[29] J. Weidlein, U. Müller, K. Dehnicke, *Schwingungsfrequenzen II – Nebengruppenelemente*, 1. Auflage, Georg-Thieme-Verlag, Stuttgart, New York **1986**.

Manuscript received: March 25, 2022
Revised manuscript received: May 23, 2022

